

Do final state interactions obscure short range correlation effects in quasielastic $A(e, e'p)$ scattering ?

A.Bianconi¹⁾, S.Jeschonnek²⁾, N.N.Nikolaev^{2,3)}, B.G.Zakharov³⁾

¹⁾*Dipartimento di Fisica Nucleare e Teorica, Università di Pavia, and Istituto Nazionale di Fisica Nucleare, Sezione di Pavia, Pavia, Italy*

²⁾*IKP(Theorie), Forschungszentrum Jülich GmbH, D-52425 Jülich, Germany*

³⁾*L.D.Landau Institute for Theoretical Physics, GSP-1, 117940, ul.Kosygina 2, V-334 Moscow, Russia*

A b s t r a c t

Are short range correlations in the ground state of the target nucleus (initial state correlations ISC) observable in experiments on quasielastic $A(e, e'p)$ scattering at large missing momentum p_m ? Will the missing momentum spectrum observed at CEBAF be overwhelmed by final state interactions of the struck proton? Taking the ${}^4\text{He}$ nucleus with a realistic model wave function for a testing ground, we present a full calculation of the missing momentum distribution in inclusive ${}^4\text{He}(e, e'p)$ scattering. We find a complex interplay and strong quantum-mechanical interference of FSI and ISC contributions to scattering at large p_m , with drastic change of the interference pattern from the (anti)parallel to transverse kinematics. We show that in all the kinematical conditions, for missing momenta $p_m \gtrsim 1 \text{ fm}^{-1}$, quasielastic scattering is dominated by FSI effects and the sensitivity to details of the nuclear ground state is lost. The origin of the FSI dominance is well understood and can be traced back to the anisotropic behaviour of FSI which is long ranged in the longitudinal direction and short ranged in the transverse direction in the opposite to the short ranged ground state correlations.

PACS: 25.30Fj, 24.10Eq

1 Introduction

Investigation of short-distance nucleon-nucleon interaction (initial state two-nucleon correlations (ISC)) in the nuclear medium is considered one of the principal goals of experiments on quasielastic $A(e, e'p)$ scattering at large missing momentum p_m [1]. Although the principal ideas and motivations for such experiments go back to Gottfried's classic works of the early 60's ([2], see also [3, 4]), they are only becoming feasible at a new generation of high luminosity, continuous beam, electron facilities (CEBAF, AmPS, MAMI, Bates). Of special importance is a new domain of large (e, e') momentum transfer squared Q^2 attainable at CEBAF [5], because for the first time the kinetic energy $T_{kin} \approx Q^2/2m_p$ of the struck proton will be high enough to exhaust the missing energy spectrum.

The experimentally measured p_m distribution is distorted by final state interaction (FSI) of the struck proton in the target nucleus debris. Are these final state interactions strong or do they just lead to small corrections to the ISC contribution to large- p_m phenomena? The answer to this pressing question and the mere possibility of the theoretical interpretation of the forthcoming CEBAF high- Q^2 experimental data on large p_m in terms of the ground state correlation effects requires the quantitative understanding of FSI effects. Several aspects of FSI in the high energy regime of CEBAF experiments have already been discussed in [6, 7, 8, 9, 10, 11, 12] with the important and disturbing finding that FSI effects completely take over and make the large- p_m behaviour of the experimentally observed missing momentum distribution drastically different from the single-particle momentum distribution (SPMD) in the ground state of the target nucleus. FSI effects were found to be strong in even such a dilute nucleus as the deuteron [10, 12]. It is obvious that at large $Q^2 \gtrsim (1 - 2) GeV^2$ and large $T_{kin} \approx Q^2/2m_p$, the conventional potential model description of FSI becomes impractical. The major point is that the very nature of nucleon-nucleon scattering changes from the purely elastic, potential scattering at low energies to a strongly absorptive, diffractive small angle scattering at $T_{kin} \gtrsim (0.5 - 1) GeV$. In this diffractive regime, Glauber's multiple scattering theory [13] becomes a natural framework for quantitative description of FSI and leads to several

important new effects in the calculation of FSI-modified one-body density matrix and missing momentum distribution in $A(e, e'p)$ scattering, which are missed in the conventional DWIA.

In our recent publication [9] we have given a simple classification and evaluation of the leading ISC and FSI contributions to the missing momentum distribution in ${}^4\text{He}(e, e'p)$. We also pointed out the numerically very substantial novel effects of quantum-mechanical interference between ISC and FSI terms and of the slowly decreasing FSI-induced tail of the missing momentum distribution in longitudinal kinematics, both of which defy the semiclassical description (for a detailed discussion of the latter effect in $A(e, e'p)$ scattering on heavier nuclei see [11]). The finding [9] of dominant pure FSI and large FSI-ISC interference effects in the leading contributions to the missing momentum distribution make a complete analysis of FSI and ISC effects for ${}^4\text{He}(e, e'p)$ scattering a pressing issue. In this communication, we report the results from such an exploratory study of the missing momentum distribution over the whole range of the missing momentum \vec{p}_m , starting with the realistic Jastrow correlated wave function and with the Glauber theory multiple scattering expansion for final state interaction of the struck proton with the spectator nucleons. Such an analysis is called upon for several reasons. On the one hand, ${}^4\text{He}$ is a simple enough nucleus in which the missing momentum distribution can be calculated to all orders in the FSI and pair correlation function, although such a calculation is quite a formidable task. Such a calculation is indispensable for understanding to which extent the FSI-modified missing momentum distribution, measured in $A(e, e'p)$ scattering, allows a reliable extraction of the SPMD and of the short range correlation effects in the ground state of the target nucleus. On the other hand, despite being a four-body system, ${}^4\text{He}$ is a high density nucleus, and there are good reasons to believe that an exhaustive analysis of FSI effects in ${}^4\text{He}$ gives a good guidance to significance of FSI effects in heavier nuclei. Finally, such an analysis allows to test how much nuclear surrounding changes predictions from generally accepted approximations, for instance, the dominance [14] of the large- p_m distributions by the quasi-deuteron configurations in the nuclear medium. The case for principal FSI effects is solid and the generality of our principal conclusions is not limited by

the model wave functions, the somewhat simplified functional form of which was motivated by a pressing necessity to circumvent the enormous complexity of numerical calculations.

The main conclusion of the present study is that distortions of the missing momentum distribution by final state interactions are very strong over the whole phase space and make an unambiguous, model independent, extraction of the large- p_m component of the SPMD from the experimental data on $A(e, e'p)$ scattering hardly possible, perhaps impossible altogether. The origin of this FSI dominance and parameters which control this dominance, are well understood. We also comment on the determination of nuclear transparency, on the accuracy of the quasi-deuteron approximation, on the rôle of FSI effects in a comparison of the large- p_m spectra for the deuteron and ${}^4\text{He}$ targets and on implications of FSI effects for the γ -scaling analysis. The analysis we report here suggests unequivocally an even stronger dominance of FSI effects in $A(e, e'p)$ scattering in heavier nuclei.

2 Missing momentum distribution: kinematics and definitions

We wish to focus on FSI effects, and for the sake of simplicity we consider the longitudinal response and treat the photon as a scalar operator. Then, following the usual procedure of factoring out the ep scattering cross section [15, 16], the experimentally measured $A(e, e'p)$ coincidence cross section can be represented in the form

$$\frac{d\sigma}{dQ^2 d\nu dp d\Omega_p} = K |M_{ep}|^2 S(E_m, \vec{p}_m, \vec{p}). \quad (1)$$

Here K is a kinematical factor, M_{ep} is the ep elastic scattering amplitude, ν and \vec{q} are the (e, e') energy and momentum transfer, $Q^2 = \vec{q}^2 - \nu^2$, the struck proton has a momentum \vec{p} and energy $E(p) = T_{kin} + m_p$, and the missing momentum and the missing energy are defined as $\vec{p}_m = \vec{q} - \vec{p}$ and $E_m = \nu + m_p - E(p) - T_{kin}(A - 1)$ (where $T_{kin}(A - 1)$ is the kinetic energy of the undetected $(A - 1)$ residual system). Hereafter, the z -axis is chosen along the (e, e') momentum transfer \vec{q} . The spectral function $S(E_m, \vec{p}_m, \vec{p})$ can be written

in terms of the nuclear reduced amplitudes \mathcal{M}_f as (for instance, see [17])

$$S(E_m, \vec{p}_m) = \sum_f |\mathcal{M}_f|^2 \delta(\nu + m_p - E(p) - E_m). \quad (2)$$

For the longitudinal response, the reduced nuclear amplitude for the exclusive process ${}^4He(e, e'p)A_f$ equals

$$\mathcal{M}_f = \int d\vec{R}_1 d\vec{R}_2 d\vec{R}_3 \Psi_f^*(\vec{R}_1, \vec{R}_2) \hat{S}(\vec{r}_1, \dots, \vec{r}_4) \Psi(\vec{R}_1, \vec{R}_2, \vec{R}_3) \exp(i\vec{p}_m \vec{R}_3). \quad (3)$$

Here $\Psi(\vec{R}_1, \vec{R}_2, \vec{R}_3)$ and $\Psi_f(\vec{R}_1, \vec{R}_2)$ are wave functions of the target 4He nucleus and of the specific 3-body final state A_f , which are conveniently described in terms of the Jacobi coordinates $\vec{R}_1 = \vec{r}_2 - \vec{r}_1$, $\vec{R}_2 = \frac{2}{3}\vec{r}_3 - \frac{1}{3}(\vec{r}_1 + \vec{r}_2)$, $\vec{R}_3 = \vec{r}_4 - \frac{1}{3}(\vec{r}_1 + \vec{r}_2 + \vec{r}_3)$ (plus $\vec{R}_{cm} = \frac{1}{4}\sum_i \vec{r}_i \equiv 0$). Lab coordinates $\{\vec{r}_i(\vec{R}_j, \vec{R}_{cm})\}$ are also used when appropriate. The specific expression (3) for \mathcal{M}_f corresponds to the nucleon “4” of 4He being chosen for the detected struck proton. $\hat{S}(\vec{r}_1, \dots, \vec{r}_4)$ stands for the S -matrix of the FSI of the struck proton with three spectator nucleons.

The calculation of the full FSI-modified spectral function $S(E_m, \vec{p}_m)$ is a separate problem, which goes beyond the scope of the present communication. In this exploratory study of the salient features of FSI, we focus on the inclusive missing momentum spectrum of protons in ${}^4He(e, e'p)$ scattering in quasielastic kinematics

$$W(\vec{p}_m) = \frac{1}{(2\pi)^3} \int dE_m S(E_m, \vec{p}_m) = \frac{1}{(2\pi)^3} \sum_f |\mathcal{M}_f|^2 \quad (4)$$

Evidently, having the high kinetic energy of the struck proton T_{kin} is important for exhausting the missing energy spectrum which at large p_m is expected to extend to particularly high E_m [6]. This for the first time becomes possible in the CEBAF range of T_{kin} . The sum over all the allowed final states A_f for the three undetected nucleons can be performed making use of the closure relation

$$\sum_f \Psi_f(\vec{R}_1', \vec{R}_2') \Psi_f^*(\vec{R}_1, \vec{R}_2) = \delta(\vec{R}_1 - \vec{R}_1') \delta(\vec{R}_2 - \vec{R}_2'). \quad (5)$$

This leads to the missing momentum distribution

$$W(\vec{p}_m) = \frac{1}{(2\pi)^3} \int d\vec{R}_3' d\vec{R}_3 \rho(\vec{R}_3, \vec{R}_3') \exp[i\vec{p}_m(\vec{R}_3 - \vec{R}_3')], \quad (6)$$

where

$$\rho(\vec{R}_3, \vec{R}_3') = \int d\vec{R}_1 d\vec{R}_2 \Psi^*(\vec{R}_1, \vec{R}_2, \vec{R}_3') S^\dagger(\vec{r}_1', \dots, \vec{r}_4') S(\vec{r}_1, \dots, \vec{r}_4) \Psi(\vec{R}_1, \vec{R}_2, \vec{R}_3) \quad (7)$$

is the FSI-modified one-body density matrix (OBDM). In the PWIA, when $\hat{S}(\vec{r}_1, \dots, \vec{r}_4) = 1$, eq. (7) reduces to the standard one-body density matrix of a nucleus and eq. (6) gives the familiar SPMD $N_F(p_m)$, also often referred to as the PWIA missing momentum distribution. Extensive studies of $N_F(p_m)$ are available in the literature ([17, 18] and references therein, see also the monograph [19]).

The main goal of this paper is to investigate the influence of FSI on, and the interplay of FSI and ISC effects in, the missing momentum distribution $W(\vec{p}_m)$, in particular at large missing momenta. The calculation of a realistic 4He wave function is a field of its own. An accurate incorporation of FSI effects into the calculation of the momentum distribution $W(\vec{p}_m)$, Eq. (6), is a numerically very involved problem. For this reason, in this exploratory study of FSI effects, we confine ourselves to a simple, yet realistic, parameterization of the wave function, which allows a semi-analytic evaluation of $W(\vec{p}_m)$. Namely, we take the popular Ansatz consisting of a harmonic oscillator mean field wave function Ψ_o and Jastrow correlation factor \hat{F} to allow for the ISC effects,

$$\Psi(\vec{R}_1, \vec{R}_2, \vec{R}_3) \equiv \hat{F} \Psi_o(\vec{R}_1, \vec{R}_2, \vec{R}_3), \quad (8)$$

where

$$\hat{F} \equiv \prod_{i < j}^4 [1 - C(\vec{r}_i - \vec{r}_j)], \quad (9)$$

$$\Psi_o \propto \exp \left[-\frac{1}{2R_o^2} \sum_i^4 \vec{r}_i^2 \right] = \exp \left[-\frac{1}{4R_o^2} \left(\vec{R}_1^2 + 3\vec{R}_2^2 + \frac{3}{2}\vec{R}_3^2 \right) \right] \quad (10)$$

and

$$C(r) = C_o \exp \left(-\frac{r^2}{2r_c^2} \right). \quad (11)$$

For a hard core repulsion $C_o = 1$, for a soft core $C_o < 1$. In the literature, one usually considers the correlation radius $r_c \approx 0.5\text{-}0.6$ fm [18, 19, 20, 21, 22]. The radius R_o of the oscillator wave function can be determined from the charge radius of the 4He , from which one must subtract the contribution from the finite charge radius of the proton.

For instance, for a hard core repulsion, $C_o = 1$, and $r_c = 0.5$ fm, the experimentally measured charge radius of the ${}^4\text{He}$ [23] is reproduced with $R_o = 1.29$ fm. Notice, that the "correlation volume" r_c^3 is a very small fraction of the volume of a nucleus and we have the strong inequality $(r_c/R_o)^3 \ll 1$.

3 Short range correlations and single particle momentum distribution

In order to set up a background, we start with a discussion of the short range correlation effects in the SPMD $N(\vec{p}_m)$. Here one has to evaluate the conventional OBDM

$$\rho(\vec{R}_3, \vec{R}_3') = \int d\vec{R}_1 d\vec{R}_2 \Psi_o^*(\vec{R}_1, \vec{R}_2, \vec{R}_3') \hat{F}^\dagger(\vec{r}_1' \dots, \vec{r}_4') \hat{F}(\vec{r}_1, \dots, \vec{r}_4) \Psi_o(\vec{R}_1, \vec{R}_2, \vec{R}_3) \quad (12)$$

The product of the Jastrow functions in (12) can be expanded as

$$\begin{aligned} \hat{F}^\dagger \hat{F} &= \prod_{i < j}^4 [1 - C^\dagger(\vec{r}_i' - \vec{r}_j')] [1 - C(\vec{r}_i - \vec{r}_j)] = \\ &1 - \sum_{i < j} [C^\dagger(i' - j') + C(i - j)] + \sum C^\dagger C + \sum C^\dagger C^\dagger + \sum C C + \dots \end{aligned} \quad (13)$$

Altogether there are 2^{12} terms in the integrand of the OBDM in Eq. (12), but with the considered Ansatz wave function it is possible to carry out all the integrations in the OBDM and in the SPMD analytically. Here we present a brief summary of main effects of short range correlations in the SPMD (for the related earlier works see [18, 19, 20], the more refined form of the above approximation known as the correlated basis function theory is widely being applied to SPMD in heavier nuclei ([22] and references therein)).

To the zeroth order in the correlation function, one finds the long ranged ¹ OBDM

$$\rho_0(\vec{R}, \vec{R}') = w_1 \frac{27}{512} \frac{1}{\pi^3} \frac{1}{R_o^6} \exp\left(-\frac{3}{8R_o^2} (\vec{R}^2 + \vec{R}'^2)\right) \quad (14)$$

¹ Hereafter, "long ranged" refers to functions which change on the scale of the ${}^4\text{He}$ radius R_o , while "short ranged" refers to functions which change on the scale of the short range correlation radius r_c and the radius of the final state proton-nucleon interaction b_0 .

(where we have introduced $\vec{R} \equiv \vec{R}_3$ and $\vec{R}' \equiv \vec{R}'_3$ for brevity) and the steeply decreasing SPMD

$$N(1; \vec{p}_m) = w_1 \exp\left(-\frac{4}{3}R_o^2 p_m^2\right), \quad (15)$$

falling off rapidly for momenta larger than the Fermi momentum $k_F \sim 1/R_0$. (Hereafter $N(1; \vec{p}_m)$, $N(C; \vec{p}_m)$, ... indicate the contributions to $N(\vec{p}_m)$ coming from the "1", "C", ... terms in the expansion (13)). Note that in any PWIA calculation, with or without correlations, the SPMD is isotropic and depends only on $|\vec{p}_m|$.

The higher order terms in C, C^\dagger in (13) can be considered as "interactions" which modify the OBDM $\rho_0(\vec{R}, \vec{R}')$ of the mean field approximation. This is shown schematically in Fig. 1. The first order corrections to $\rho(\vec{R}, \vec{R}')$ and $N(\vec{p}_m)$ come from the terms which are linear in $C(\vec{r}_i - \vec{r}_j)$ and $C^\dagger(\vec{r}_i' - \vec{r}_j')$. Leading corrections to $N(\vec{p}_m)$, which decrease with p_m substantially slower than the zeroth order term (15), come from interactions of Fig. 1a, which affect only one of the trajectories in the calculation of the OBDM. One can easily verify that the corresponding corrections to the OBDM are long-ranged, and lead to the contribution to SPMD of the form

$$N(C^\dagger + C; \vec{p}_m) \approx -6w_1 C_0 \sqrt{\frac{27}{125}} \left(\frac{r_c}{R_o}\right)^3 \exp\left(-\frac{4}{5}R_o^2 p_m^2\right). \quad (16)$$

For the sake of brevity, we don't show here and in the following equations correction factors $[1 + \mathcal{O}(r_c^2/R_o^2)]$ to the slope and the normalization factors. Of course, those factors are included in our calculations. Notice, that the normalization in (16) contains the small factor $(r_c/R_o)^3$. Notice also the destructive interference between the $N(1; \vec{p}_m)$ and $N(C^\dagger + C; \vec{p}_m)$, which becomes stronger with increasing p_m , because the latter has a smaller slope of the \vec{p}_m^2 dependence than the former.

The driving contributions to the short ranged component of the OBDM and the related large- p_m component of the SPMD come from the three identical terms of the form $C^\dagger(\vec{r}_4' - \vec{r}_i')C(\vec{r}_4 - \vec{r}_i)$. They produce a short range interaction of the type shown in Fig. 1b between the two trajectories which enter the calculation of the OBDM and lead to a short ranged component of the OBDM of the form

$$\rho(C^\dagger C, \vec{R}, \vec{R}') = 3 \int d^3\vec{R}_1 d^3\vec{R}_2 \Psi_o \Psi'_o C^\dagger(\vec{r}_3' - \vec{r}_4') C(\vec{r}_3 - \vec{r}_4)$$

$$\approx w_1 C_o^2 \frac{1}{\pi^3} \sqrt{\frac{3^{11}}{2^{21}}} \frac{r_c^3}{R_o^9} \exp\left(-\frac{1}{4r_c^2} (\vec{R} - \vec{R}')^2 - \frac{9}{8R_o^2} (\vec{R}^2 + \vec{R}'^2)\right). \quad (17)$$

The resulting large- p_m component of the SPMD directly probes the correlation function $C(\vec{R})$:

$$\begin{aligned} N(C^\dagger C; \vec{p}_m) &\approx w_1 C_o^2 \frac{1}{2\pi^3} \frac{1}{R_o^6} \sqrt{\frac{243}{512}} \left| \int d^3 \vec{r} C(\vec{r}) \exp(i\vec{p}_m \vec{r}) \right|^2 \\ &= N(C^\dagger C; \vec{p}_m) \approx w_1 C_o^2 \sqrt{\frac{243}{512}} \left(\frac{r_c}{R_o}\right)^6 \exp(-r_c^2 p_m^2). \end{aligned} \quad (18)$$

(For the sake of brevity, we suppressed here the correction factors $[1 + \mathcal{O}(r_c/R_o)^2]$ to the slope of p_\perp^2 dependence and the total normalization.) Notice, that the short ranged component of the OBDM is proportional to the correlation volume, whereas the large- p_m tail of the SPMD contains the small normalization factor $\propto (r_c/R_o)^6$.

The correlated pair of nucleons is often treated as a quasi-deuteron ([17] and references therein). Indeed, Eq. (18) resembles the momentum distribution in the quasi-deuteron with the short-range correlation function playing the rôle of the wave function of the quasideuteron (for the recent analysis of ${}^2H(e, e'p)$ scattering see [10, 12]).

The terms $\propto CC, C^\dagger C^\dagger$ in expansion (13) correspond to interactions which involve only one of the trajectories in $\rho(\vec{R}, \vec{R}')$ and give a long ranged contribution to the OBDM and a steeply decreasing contribution to the SPMD $N(\vec{p}_m)$, similar to (15),(16). The above analysis can easily be extended to still higher order effects in the correlation function. For instance, the cyclic terms of the form $C^\dagger(\vec{r}_4 - \vec{r}_3)C(\vec{r}_4' - \vec{r}_2)C(\vec{r}_2 - \vec{r}_3)$ also lead to a short-range interaction between the two trajectories in the OBDM, as shown in Fig. 1c. For the presence of the extra link in the 4-2-3 chain, though, the corresponding interaction range is larger than in the diagram of Fig. 1b, and the resulting contribution from such cyclic terms to the SPMD has a p_m dependence steeper than in Eq. (18):

$$N\left([C^\dagger CC + C^\dagger C^\dagger C]_{cyclic}; \vec{p}_m\right) \approx -6w_1 C_o^3 \sqrt{\frac{1}{8}} \left(\frac{r_c}{R_o}\right)^9 \exp\left(-\frac{3}{2}r_c^2 p_m^2\right) \quad (19)$$

However, numerically more important are the non-cyclic third order terms of the form $C^\dagger(\vec{r}_4' - \vec{r}_i')C(\vec{r}_4 - \vec{r}_i)C^\dagger(\vec{r}_j - \vec{r}_k)$, which have a slow p_m^2 dependence equal to that of the

leading $C^\dagger C$ contribution (17) but are of the opposite sign:

$$N([C^\dagger CC + C^\dagger C^\dagger C]_{non-cyclic}; \vec{p}_m) \approx -10w_1 C_o^3 \sqrt{\frac{243}{512}} \left(\frac{r_c}{R_o}\right)^9 \exp(-r_c^2 p_m^2). \quad (20)$$

Such a destructive interference between the $C^\dagger CC + C^\dagger C^\dagger C$ and $C^\dagger C$ contributions to the SPMD demonstrates a well understood suppression of interaction between any pair of nucleons for the repulsive correlation with surrounding nucleons, for more discussion see below.

The above considerations are illustrated by the numerical results shown in Figs.2,3,4,5. The sensitivity of the SPMD to short range correlations is obvious from a comparison in Fig.2 of the mean field distribution, $C_o = 0$, with the soft core correlation $C_o = 0.5$ and the hard core correlation $C_o = 1$. For $C_o = 0$, the mean field SPMD (15) falls off rapidly for $p_m \gtrsim k_F \sim 1/R_o$. Once the short range correlations are included, the large- p_m tail builds up, with the strength which closely follows the law $\propto C_o^2$. The effect of destructive interference between the mean field SPMD (15) and the lowest order ISC contribution (16) is obvious at intermediate $p_m \sim k_F$. The interference effect rises with the correlation strength C_o . One usually considers $r_c \sim 0.5$ fm, but the exact value of the correlation radius r_c is not known precisely [18, 20, 21]. According to the estimate (18), the ISC contribution to SPMD rises steeply, $\propto r_c^6$, with the correlation radius r_c . However, at large values of p_m where the short range correlation component takes over the mean field component, the suppression by the factor $\exp(-r_c p_m^2)$ is quite significant and the residual sensitivity to the variation of r_c is weaker than $\propto r_c^6$. This is illustrated by Fig.3, where we compare the SPMDs for $r_c = 0.5$ fm and $r_c = 0.6$ fm.

Above we cited the explicit form of leading terms in the SPMD. The rate of convergence of the expansion in powers of the correlation function is of great interest on its own. For instance, the large- p_m tail of the SPMD is often discussed in terms of the quasi-deuteron configurations, neglecting the effect of the nuclear surrounding. If this were a good approximation, then one would have expected a universality of the large- p_m SPMDs for all nuclei. The accuracy of this approximation can be judged from Fig.4, where we present the results for $N(p_m)$ including all terms up to the second order, i.e., $C^\dagger C^\dagger +$

$C^\dagger C + CC$ (dotted line), to the fourth order (dashed line), to the sixth order (dash-dotted line), to the eighth order (double-dotted line), and the full expansion (13) up to the twelfth order terms (solid line) is plotted. (Truncation of an expansion at lowest odd orders of the correlation function can result in $N(\vec{p}_m)$ which is not positive valued). All the different single-particle momentum distributions are normalized to unity. Although the shape of the SPMD does not change qualitatively, we find a substantial, $\sim 40\%$, renormalization of the lowest-order quasi-deuteron contribution to $N(\vec{p}_m)$ by effects of the nuclear environment. This shows that the large- p_m behaviour of the SPMD is sensitive to details of the nuclear wave function and a quasi-deuteron universality of the SPMD at large p_m is though a reasonable, but not a very accurate, approximation. The effect of higher order corrections is evident from the form of the Jastrow correlation factor: the mutual repulsion from surrounding nucleons suppresses the probability of short distance interaction between any pair of nucleons in the nucleus, cf. Eqs. (29) and (30,31). The effect of higher order terms is particularly important at intermediate values of $p_m \sim k_F \sim 1/R_0$, where our model SPMD develops a slight minimum. Our model wave function contains only those many nucleon correlation effects, which are reducible to higher orders in the pair correlation function. The fact that terms up to sixth order are non-negligible at large p_m , suggests that the presently poorly known pair-irreducible multinucleon correlations can also contribute to the SPMD at large momentum.

Fig. 2 shows that the shape of the SPMD changes with the correlation strength in a nontrivial way. In Fig.5 we present the renormalization factor

$$R_C(p_m) = \frac{N(C_0 = 1; p_m)}{N(C_0 = 0; p_m)}, \quad (21)$$

which expands to greater detail the difference between the mean field and correlated distributions. At large p_m this ratio blows up, but at intermediate $p_m \lesssim k_F$ it has a nontrivial behaviour: The short range correlation effects *enhance, rather than suppress*, the SPMD and lead to $R_C(p_m) > 1$ at small p_m , the extra strength at large p_m due to short range correlations, comes from a depletion of SPMD at $p_m \sim k_F$, rather than from the region of $p_m \sim 0$.

There are no direct experimental data on the SPMD in ${}^4\text{He}$ to compare our results with. Our model SPMD $N(\vec{p}_m)$ is close to the results from the recent Monte Carlo calculation [24] and the y -scaling analysis [17].

4 Final state interaction effects.

At the large Q^2 of interest in the CEBAF experiments, FSI can be described by Glauber theory. Defining transverse and longitudinal components $\vec{r}_i \equiv (\vec{b}_i, z_i)$ and $\vec{R}_i \equiv (\vec{B}_i, Z_i)$ we can write

$$\hat{S}(\vec{r}_1, \dots, \vec{r}_4) = \prod_{i=1}^3 \left[1 - \theta(z_i - z_4) \Gamma(\vec{b}_4 - \vec{b}_i) \right], \quad (22)$$

where $\Gamma(\vec{b})$ is the profile function of the nucleon-nucleon scattering

$$\Gamma(\vec{b}) \equiv \frac{\sigma_{tot}(1 - i\rho)}{4\pi b_o^2} \exp \left[-\frac{\vec{b}^2}{2b_o^2} \right] \quad (23)$$

(ρ is the ratio of the real to imaginary part of the forward elastic scattering amplitude). The Glauber formalism describes quite well nucleon-nucleus scattering at energies above 500 MeV, even at angles as large as 30° at 500 MeV (for a review see [25]). At $T_{kin} \sim 1\text{GeV}$, the experimental data on pN scattering give $b_o \approx 0.5\text{fm}$, $\sigma_{tot} \approx 40\text{mb}$ and $\rho = 0.33$ [25, 26, 27]. These parameters of pN scattering vary only very weakly over the GeV energy range relevant to the CEBAF experiments. This weak dependence of FSI on the kinetic energy of the proton has actually been used in the application of closure to derivation of Eq. (7) for the FSI-modified OBDM, in which we neglected the dependence of the FSI operator $S(\vec{r}_1, \dots, \vec{r}_4)$ on the missing energy E_m .

Combining together the FSI and the Jastrow correlation factors, we can write down the FSI-modified density matrix as

$$\begin{aligned} \rho(\vec{R}_3, \vec{R}_3') &= \int d\vec{R}_1 d\vec{R}_2 \\ &\times \Psi_o^*(\vec{R}_1, \vec{R}_2, \vec{R}_3') \hat{F}^\dagger(\vec{r}_1', \dots, \vec{r}_4') \hat{S}^\dagger(\vec{r}_1', \dots, \vec{r}_4') \hat{S}(\vec{r}_1, \dots, \vec{r}_4) \hat{F}(\vec{r}_1, \dots, \vec{r}_4) \Psi_o(\vec{R}_1, \vec{R}_2, \vec{R}_3). \end{aligned} \quad (24)$$

The operator $\hat{F}^\dagger \hat{S}^\dagger \hat{S} \hat{F}$ which emerges in (24) can be expanded as

$$\hat{F}^\dagger \hat{S}^\dagger \hat{S} \hat{F} = \prod_{i < j}^4 \left[1 - C^\dagger(\vec{r}_i' - \vec{r}_j') \right] \left[1 - C(\vec{r}_i - \vec{r}_j) \right]$$

$$\begin{aligned}
& \times \prod_{i \neq 4} [1 - \theta(z'_i - z'_4) \Gamma^\dagger(\vec{b}'_4 - \vec{b}'_i)] [1 - \theta(z_i - z_4) \Gamma(\vec{b}_4 - \vec{b}_i)] = \\
1 - \sum_{i < j} [C^\dagger + C] - \sum_{i \neq 4} [\Gamma^\dagger + \Gamma] + \sum [C^\dagger \Gamma + C \Gamma^\dagger] + \sum C^\dagger C + \sum \Gamma^\dagger \Gamma + \dots \quad (25)
\end{aligned}$$

The rôle of the FSI terms in the expansion (25) is very similar to that of the short-range correlation terms. There are interactions which only involve one of the trajectories in the FSI-modified OBDM, there are terms of the form $\theta(z'_i - z'_4) \theta(z_i - z_4) \Gamma^\dagger(\vec{b}'_4 - \vec{b}'_i) \Gamma(\vec{b}_4 - \vec{b}_i)$, which lead to an interaction between the two trajectories etc. There also emerges a novel kind of an interaction between the two trajectories of the form $C^\dagger(\vec{b}'_4 - \vec{b}'_i) \Gamma(\vec{b}_4 - \vec{b}_i)$ (plus its hermitian conjugate and higher order short ranged interactions), which is due to the quantum-mechanical interference between the initial state correlations and final state interactions [9]. The rôle of different terms in the expansion (25) will be discussed in more detail below.

The salient features of FSI stem from the observation that the Glauber operator $\theta(z_i - z_4) \Gamma(\vec{b}_4 - \vec{b}_i)$ is a short ranged function of the transverse separation $\vec{b}_4 - \vec{b}_i$ and a long ranged function of the longitudinal separation $\theta(z_i - z_4)$. This angular anisotropy of the FSI operator leads to an angular anisotropy of the missing momentum distribution $W(\vec{p}_m)$ and in the further discussion we decompose the missing momentum into transverse and longitudinal components $\vec{p}_m = (\vec{p}_\perp, p_{m,z})$.

In the range of kinetic energies of the proton typical of the CEBAF range of Q^2 , the transverse range of FSI, $b_0 \approx 0.5$ fm, is numerically very close to the correlation radius: $b_0 \sim r_c$. Now we briefly recapitulate the most striking effects of FSI terms in the expansion (25), following the classification developed in [9].

The terms linear in Γ^\dagger and Γ correspond to an interaction with one of the two trajectories in the OBDM as shown in Fig. 6a. As such, they lead to a long ranged contribution to the OBDM and to a contribution $W(\Gamma^\dagger + \Gamma; \vec{p}_m)$ to the FSI-modified missing momentum distribution of the form very similar to $N(C^\dagger + C; \vec{p}_m)$ of Eq. (14), but with the normalization typical of the Glauber multiple scattering theory [13, 28]

$$Y \sim \frac{\sigma_{tot}}{4\pi b_0^2} \cdot \left(\frac{b_0}{R_0} \right)^2 = \frac{\sigma_{tot}}{4\pi R_0^2}, \quad (26)$$

which is larger than the normalization in (16) by a factor of the form

$$\frac{W(\Gamma^\dagger + \Gamma; \vec{p}_m)}{N(C^\dagger + C; \vec{p}_m)} \sim \left(\frac{\sigma_{tot}}{4\pi b_0^2} \right) \cdot \left(\frac{b_0}{R_0} \right)^2 \cdot \left(\frac{R_0}{r_c} \right)^3 \cdot \frac{1}{C_0} \sim \frac{R_0}{r_c} \cdot \frac{1}{C_0} \gg 1. \quad (27)$$

Here we made use of the fact that $\sigma_{tot} \sim 4\pi b_0^2$ and $b_0 \sim r_c$. The enhancement factor $\sim R_0/r_c$ in (27) derives from the fact that the Glauber operator is a long ranged function of the longitudinal separation in contrast to the short ranged correlation function and is the simplest demonstration that FSI effects in the missing momentum distribution are more important than the ISC effects. Eq. (27) gives an estimate of the relative normalizations of the two components of the missing momentum distribution. The transverse momentum dependence of both components is essentially identical. For the presence of the θ -function in the Glauber operator, the $p_{m,z}$ dependence of $W(\Gamma; \vec{p}_m)$ can not be written down in a simple analytical form (one can derive an involved and not very enlightening expression in terms of an error function of a complex argument); what is important is that it is a steeply decreasing function of $p_{m,z}$ on the scale k_F .

An analysis of higher order effects proceeds very similarly. The driving short ranged FSI contribution to the OBDM and to the large- p_m tail of the missing momentum distribution $W(\vec{p}_m)$ comes from diagrams of the type shown in Fig. 6b which correspond to terms $\propto \Gamma^\dagger(\vec{b}_4 - \vec{b}_i)\Gamma(\vec{b}_4 - \vec{b}_i)$ in the expansion (25). Suppressing for a while the $p_{m,z}$ dependence and making use of the strong inequality $(b_0/R_0)^2 \ll 1$, in close similarity to $N(C^\dagger C; \vec{p}_m)$ we find

$$W(\Gamma^\dagger \Gamma; \vec{p}_m) \propto \left| \int d^2 \vec{B} \Gamma(\vec{B}) \exp(i\vec{p}_\perp \vec{B}) \right|^2 = 4\pi \frac{d\sigma_{el}}{dp_\perp^2} = \frac{1}{4} \sigma_{tot}^2 (1 + \rho^2) \exp(-b_o^2 p_\perp^2). \quad (28)$$

The result that this particular contribution to the transverse missing momentum distribution is proportional to the differential cross section of elastic pN scattering $d\sigma_{el}/dp_\perp^2$, is self-explanatory and the effect of $\Gamma^\dagger \Gamma$ interaction admits a quasiclassical interpretation as an incoherent elastic rescattering of the struck proton on spectator nucleons. The still higher order terms of the form $\propto \Gamma^\dagger(\vec{b}_4 - \vec{b}_i)\Gamma(\vec{b}_4 - \vec{b}_i)\Gamma^\dagger(\vec{b}_4 - \vec{b}_k)\Gamma(\vec{b}_4 - \vec{b}_k)$ lead to a second order short ranged interaction between the trajectories in the FSI-modified OBDM. The transverse momentum dependence of such a contribution to $W(\vec{p}_m)$ also admits a semi-classical form of the convolution of differential cross sections of consecutive incoherent

elastic scatterings and

$$W(\Gamma^\dagger\Gamma\Gamma^\dagger\Gamma; \vec{p}_m) \propto Y^2 \exp\left(-\frac{1}{2}b_o^2 p_\perp^2\right). \quad (29)$$

The $\propto (b_0/R_0)^2$ corrections to the slopes in (28) can readily be derived and correspond very qualitatively to a slight smearing of the elastic scattering cross section due to the -compared to the momentum transfer in elastic pN scattering- small initial Fermi motion of the struck proton and the spectator nucleon (for a critical discussion of semiclassical considerations see [11]).

Because of $b_o \approx r_c$ in the CEBAF range of Q^2 , the short ranged $C^\dagger C$ and $\Gamma^\dagger\Gamma$ interactions between the two trajectories in $\rho(\vec{R}, \vec{R}')$ lead to $W(C^\dagger C; \vec{p}_m) = N(C^\dagger C; \vec{p}_m)$ and $W(\Gamma^\dagger\Gamma; \vec{p}_m)$ components with very similar p_\perp dependence. In close similarity to Eq. (27), the overall normalization is substantially larger for the FSI term. A comparison of the two components at $p_{m,z} = 0$ gives

$$\frac{W(\Gamma^\dagger\Gamma; \vec{p}_m)}{W(C^\dagger C; \vec{p}_m)} \approx \frac{1}{C_o^2 \sqrt{6}} \cdot \left[\frac{\sigma_{tot}}{4\pi r_c^2} \right]^2 \cdot \left(\frac{R_o}{r_c} \right)^2 \sim 7 \quad (30)$$

and leads to the important conclusion that the tail of the transverse missing momentum distribution must be entirely dominated by FSI effects.

Because the FSI is long-ranged in $z_4 - z_i$, $W(\Gamma^\dagger\Gamma; \vec{p}_m)$ decreases steeply with $p_{m,z}$ on the scale $\sim k_F \sim 1/R_0$. On the one hand, this leads to a strong angular anisotropy of the elastic rescattering effect, cf. Eq. (29). On the other hand, one would have naively expected the continuation of this steep decrease of the $\Gamma^\dagger\Gamma$ contribution and the dominance of the $C^\dagger C$ correlation component (18) of the SPMD in the longitudinal kinematics at large $|p_{m,z}| \gtrsim k_F$. There are deep quantum mechanical reasons why this is not the case. The $p_{m,z}$ dependence of $W(\Gamma^\dagger\Gamma; \vec{p}_m)$ has peculiarities of its own. The θ -function, which is present in the Glauber operator, has a slowly decreasing Fourier transform at large $p_{m,z}$. The contribution from the $\Gamma^\dagger\Gamma$ interaction to the integrand of the OBDM contains the product of the θ -functions of the form $\theta(z'_i - z'_4)\theta(z_i - z_4) = \theta(z_i - z_{max})$, where

$$z_{max} = \frac{1}{2}(z_4 + z'_4) + \frac{1}{2}|z_4 - z'_4|. \quad (31)$$

The nonanalytic function $|z_4 - z'_4|$ in z_{max} gives rise to a $p_{m,z}^{-2}$ tail of the longitudinal missing momentum distribution after the calculation of the Fourier transform in $z_4 - z'_4$ (for a detailed discussion of the case of heavy nuclei see [11]). The factor $\theta(z'_i - z'_4)\theta(z_i - z_4)$ implies that the $\Gamma^\dagger\Gamma$ interaction is forbidden on the part of either one or the other of the trajectories in the calculation of the OBDM as shown schematically in Fig. 6. This ban on the $\Gamma^\dagger\Gamma$ interaction is of purely quantum-mechanical origin and the $\propto p_{m,z}^{-2}$ tail of the longitudinal missing momentum distribution defies any classical interpretation, in contrast to the strong FSI enhancement of the transverse missing momentum distribution, which admits a semiclassical interpretation to a certain extent. For the reasons explained in detail in [11], the $\Gamma^\dagger\Gamma$ interaction and the resulting $\propto p_{m,z}^{-2}$ tail of the missing momentum distribution are missed in the conventional DWIA.

Finally, still another nontrivial effect, the quantum-mechanical interference of ISC and FSI, comes from the terms $\propto C^\dagger(\vec{r}_4' - \vec{r}_i')\Gamma(\vec{b}_4 - \vec{b}_i)$ and $\propto C(\vec{r}_4 - \vec{r}_i)\Gamma^\dagger(\vec{b}_4' - \vec{b}_i')$. These and higher order cyclic and non-cyclic terms lead to a short range interaction as shown in Fig 6c in the transverse separation between the trajectories in the calculation of the OBDM (22) and to a large- p_m tail of the transverse missing momentum distribution of the form

$$w(C\Gamma^\dagger + C^\dagger\Gamma; \vec{p}_m) \propto \int d^2\vec{R} C^\dagger(\vec{R}) \exp(i\vec{p}_\perp \vec{R}) \cdot \text{Re} \int d^2\vec{B} \Gamma(\vec{B}) \exp(-i\vec{p}_\perp \vec{B}) \\ \propto \exp\left[-\frac{1}{2}(r_c^2 + b_o^2)p_\perp^2\right]. \quad (32)$$

Considering that $b_0 \sim r_c$, at large p_\perp the effects of the $C\Gamma^\dagger + C^\dagger\Gamma$ interaction are as important as those of the $C^\dagger C$ and $\Gamma^\dagger\Gamma$ interactions. Furthermore, the remarkable feature of the FSI-ISC interference term is that owing partly to numerical factors, it has a large normalization. At $p_{m,z} = 0$ we find

$$\frac{W(C\Gamma^\dagger + C^\dagger\Gamma; \vec{p}_m)}{W(\Gamma^\dagger\Gamma; \vec{p}_m)} \approx 4\sqrt{\frac{3}{5}}C_o \left(\frac{4\pi r_c^2}{\sigma_{tot}}\right) \cdot \frac{r_c}{R_o} \sim 1. \quad (33)$$

This clearly shows that the FSI-ISC interference effect is much more important than the pure ISC component of the missing momentum distribution. Notice that any semiclassical consideration would completely miss this large ISC-FSI interference effect. Furthermore,

the numerical significance of this interference effects shows that even in transverse kinematics, the semiclassical treatment of FSI misses important quantum mechanical effects and must be taken with great caution. The $p_{m,z}$ dependence of this contribution to $W(\vec{p})$ will be controlled by the long range character in the longitudinal separation of the Glauber operator.

5 Final state interaction and missing momentum distribution: the numerical results

The full calculation of the FSI-modified OBDM is quite involved, because the full expansion (24,25) for the integrand of the OBDM involves 2^{18} terms. The θ -function in the Glauber operator leads to the slow convergence of the Fourier transform and requires very tight control of numerical accuracy in the calculation of the FSI-modified missing momentum distribution, especially at large $|p_{m,z}|$. With the generic wave function, an accurate calculation of the large- p_m behaviour of $W(\vec{p}_m)$ would have required enormous computing time. Our Ansatz wave function, complemented by the usual Gaussian form of the profile function, simplifies the task greatly, because all the transverse coordinate integrations and the corresponding Fourier transform in the transverse missing momentum can be performed analytically to all orders in ISC and FSI. Only the longitudinal coordinate integrations and the corresponding Fourier transform must be performed numerically. Now we present some of the results for the missing momentum distribution $W(\vec{p}_m)$. Unless specified otherwise, all the numerical results are for the hard core correlation, $C_0 = 1$.

As the PWIA missing momentum distribution including the correlation functions is completely isotropic, any anisotropy in $W(\vec{p}_m)$ is a clear signal of FSI. In Fig. 7, we show the angular distribution of $W(\vec{p}_m)$ for different missing momenta for the full calculation with FSI (solid line) and the PWIA result (dashed line). Already at the rather low missing momentum of $p_m = 1.0 fm^{-1}$, there is a strong deviation from the isotropic PWIA behaviour. With growing missing momentum, the dip around 90° evolves through

a very asymmetric stage into a pronounced peak at $p_m \gtrsim 1.6 \text{ fm}^{-1}$, the signal of complete FSI (plus ISC-FSI interference) dominance. The evolution of the angular distribution is especially fast around $p_m \sim 1.5 \text{ fm}^{-1}$. One of the striking effects in Fig. 7 is the forward-backward asymmetry $W(p_\perp, p_z) \neq W(p_\perp, -p_z)$. This forward-backward asymmetry has its origin in the nonvanishing real parts of the $p-n$ and $p-p$ scattering amplitudes $\rho \neq 0$, leading to $\hat{S}^\dagger(\vec{b}_1, z'_1, \dots, \vec{b}_4, z'_4) \hat{S}(\vec{b}_1, z_1, \dots, \vec{b}_4, z_4) \neq \hat{S}^\dagger(\vec{b}_1, z_1, \dots, \vec{b}_4, z_4) \hat{S}(\vec{b}_1, z'_1, \dots, \vec{b}_4, z'_4)$ in the integrand of (7).

The same features of $W(\vec{p}_m)$ can be seen in the missing momentum distributions displayed for longitudinal and transverse kinematics in Fig. 8. For small missing momentum, the FSI leads to a reduction of strength, at $p_m = 0$ the PWIA distribution is depleted by $\sim 24\%$, which is about twice as large as the nuclear shadowing effect in the total $p^4\text{He}$ cross section [28]. Two mechanisms contribute to this depletion which is mostly due to the $\Gamma^\dagger + \Gamma$ terms in the expansion (25): i) attenuation of the flux of struck protons due to absorption by inelastic interaction with the spectator nucleons, ii) deflection of the struck protons by elastic scattering on the spectator nucleons. Such a semiclassical interpretation must be taken with the grain of salt, though: because of the quantum-mechanical interference effects, FSI leads to quite an involved, strongly \vec{p}_m dependent, pattern of depletion and/or enhancement of the FSI modified missing momentum distribution $W(\vec{p}_m)$ as compared to the PWIA distribution $N(\vec{p}_m)$ (see also below, section 7). With the increasing missing momentum, up to $p_m < 0.5 \text{ fm}^{-1}$, the angular distribution is almost isotropic, from $p_m = 0.5 \text{ fm}^{-1}$ on, the deviations from the isotropic PWIA behaviour grow larger. In transverse kinematics, from $p_m = 1.5 \text{ fm}^{-1}$ on, the full calculation including FSI (solid line) shows a large tail at high missing momenta, which is one order of magnitude larger than the tail of the PWIA distribution $N(p_m)$ for hard core correlations (dotted line).

The peculiarities of the Fourier transform of the θ -function factors do not show up in transverse kinematics, at $p_{m,z} = 0$. Here the rôle of the Glauber operator $\Gamma(\vec{b})$ in the evaluation of the FSI-modified OBDM is nearly identical to the rôle of the correlation function $C(\vec{r})$ in the modification of the mean-field OBDM. The only difference is in a much larger strength of FSI effects, which is the reason why $W(\vec{p}_m)$ develops a minimum at

$p_m \approx 1.4 fm^{-1}$ as compared to the minimum of the PWIA distribution at $p_m \approx 1.7 fm^{-1}$.

To this end, notice that $p_m \sim 1.4 fm^{-1}$ corresponds to a region of p_m in which the effect of short range correlations in the SPMD is still marginal. Already this observation suggests very strongly that in transverse kinematics, $\theta = 90^\circ$, the missing momentum distribution $W(\vec{p}_m)$ can only weakly depend on the short-range correlation effects in the nuclear wave function. This is indeed the case. The results shown in Fig. 9 demonstrate that, in a striking contrast to the strongly correlation dependent PWIA distribution $N(\vec{p}_m)$ of Fig. 2, the FSI-modified $W(\vec{p}_m)$ is extremely insensitive to the strength of short range correlation. Namely, even at large $p_m \gtrsim 1.5 fm^{-1}$ the missing momentum distribution $W(\vec{p}_m)$ calculated with $C_o = 1$ is only by $\sim 50\%$ larger than $W(\vec{p}_m)$ calculated with $C_o = 0$, in contrast to a difference of several orders in magnitude in the PWIA distributions for $C_o = 0$ and $C_o = 1$. This enhancement is much stronger than expected from the ISC contribution of PWIA, though. In a classical consideration, such an enhancement of $W(\vec{p}_m)$ with the correlation strength is quite counterintuitive: the classical probability of elastic rescattering of the struck proton on the spectator nucleon is higher for close configurations, which are suppressed by the hard core correlation. The found enhancement of $W(\vec{p}_m)$ from the mean field, $C_o = 0$, to the hard core correlation, $C_o = 1$, wave function must be attributed to the above discussed ISC-FSI interference effect, see Eq. (31), which is numerically larger than the effect of suppression of $\Gamma^\dagger\Gamma$ elastic rescattering contribution by the short range correlation [9]. Fig. 10 shows that the situation changes neither qualitatively nor quantitatively if the correlation radius is increased from $r_c = 0.5 fm$ to $r_c = 0.6 fm$. Thus, we are led to the conclusion that FSI is dominating completely and that it would be extremely difficult to disentangle the effects of short range correlations in the ground state of the target nucleus from the FSI-affected experimental data on $A(e, e'p)$ scattering in transverse kinematics.

Let's have a look at longitudinal kinematics, $\theta = 0^\circ$ and $\theta = 180^\circ$, to check if the situation there is more promising. In the angular distributions of Fig. 7 one can see that also in longitudinal kinematics, deviations from the PWIA behaviour are present and large. The missing momentum distributions for longitudinal kinematics displayed in

Figs.8b,c differ strongly from $W(\vec{p}_m)$ in transverse kinematics. Firstly, in the antiparallel kinematics, at $\theta = 180^\circ$, the $\approx 24\%$ nuclear depletion of $W(\vec{p}_m)$ at $p_m = 0$ goes away with increasing p_m and is superseded by nuclear enhancement at $p_m \gtrsim 1 fm^{-1}$. In parallel kinematics, at $\theta = 0^\circ$, a similar transition from nuclear depletion to nuclear enhancement takes place at $p_m \gtrsim 1.5 fm^{-1}$. This difference between the parallel and antiparallel kinematics is due to the before-mentioned forward-backward asymmetry generated by the nonvanishing value of ρ . The minimum or shoulder-like irregularity that is present in PWIA at $p_m \approx 1.7 fm^{-1}$, and which in transverse kinematics is shifted by FSI to $p_m \approx 1.4 fm^{-1}$, is washed out by the FSI in longitudinal kinematics, for both parallel and antiparallel configurations. Now, $W(\vec{p}_m)$ is decreasing monotonously.

The results for parallel kinematics, $\theta = 0^\circ$, show that the PWIA distribution $N(p_m)$ and the FSI-modified distribution $W(\vec{p}_m)$ are very close to each other for missing momenta $p_m > 2 fm^{-1}$, although $W(\vec{p}_m)$ slightly undershoots the PWIA values. Must this be taken as evidence that FSI is unimportant in parallel kinematics, at $\theta = 0^\circ$? The results shown in Figs. 9b,c do clearly demonstrate this is not the case. In parallel kinematics, Fig. 9b, $W(\vec{p}_m)$ hardly changes from the mean field, $C_0 = 0$, (dotted line) to the soft core correlation, $C_0 = 0.5$, (dashed line) to the hard core correlation, $C_0 = 1$, (solid line), which must be contrasted to a dramatic sensitivity of the SPMD to the correlation strength C_0 in the same region of large p_m . In antiparallel kinematics, for $\theta = 180^\circ$, the FSI-modified distribution $W(\vec{p}_m)$ of Fig. 9 exhibits a stronger sensitivity to short range correlations. However, this dependence on the correlation strength C_0 is quite counterintuitive, as $W(p_m)$ decreases substantially when short range correlations are switched on, remaining lower than both the PWIA distribution $N(p_m)$ and the FSI-modified distribution $W(\vec{p}_m)$ evaluated in the mean field approximation $C_0 = 0$. Notice also, that the difference between the cases of the soft core and hard core correlations in Fig 9 is much smaller than the difference between the PWIA distribution $N(\vec{p}_m)$ and the FSI-modified distribution $W(\vec{p}_m)$ for $C_0 = 1$ in Fig 8. The results for the larger correlation radius $r_c = 0.6 fm$, shown in Fig.10, are not any different from those for $r_c = 0.5$, the change of $W(\vec{p}_m)$ from $r_c = 0.5 fm$ to $r_c = 0.6 fm$ is marginal.

What actually happens in parallel and anti-parallel kinematics is a manifestation of still another strong ISC-FSI correlation effect, which in this case is connected with the real part of the pN elastic scattering amplitude. In Fig.11 we show separately the large- p_m behaviour of $W_+(p_m) = \frac{1}{2}[W(\theta = 0^\circ; p_m) + W(\theta = 180^\circ)]$, which is free of the FSI contribution linear in ρ (the terms $\propto \rho^2$ that are present in W_+ are very small). In the mean field approximation, $C_0 = 0$, the large- p_m tail of $W_+(p_m)$ is entirely due to the θ -function effects. As it was discussed in detail in [9, 10, 11], this tail is suppressed by the correlation effects, which naturally smoothes out the idealized θ -function in the Glauber operator which assumes idealized pointlike nucleons. On the other hand, the PWIA distribution at $C_0 = 1$ is numerically very close to the FSI effect at $C_0 = 0$. When both the FSI and ISC effects are included, with the increase of C_0 the rising correlation contribution compensates partly for a decrease of the FSI contribution. The net effect is a weak depletion of $W_+(p_m)$ from the mean field, $C_0 = 0$, value to the soft core correlation value at $C_0 = 0.5$. However, there is hardly any change in $W_+(p_m)$ from the soft core to hard core correlation result for $W_+(p_m)$. This is due to a certain numerical conspiracy between the correlation and FSI parameters. From the practical point of view it is important that for a weak energy dependence of the pN scattering parameters, such a conspiracy will persist over the whole range of Q^2 to be explored at CEBAF.

The substantial rôle of the real part of the pN scattering amplitude in this region of large p_m is obvious from the FSI-induced forward-backward asymmetry

$$A_{FB}(p_m) = \frac{W(\theta = 0^\circ; p_m) - W(\theta = 180^\circ; p_m)}{2W_+(p_m)}, \quad (34)$$

which is shown in Fig.12. It exhibits a strong dependence on the correlation strength and is quite large for the hard core correlation $C_0 = 1$. The forward-backward asymmetry is an intricate FSI-PWIA interference effect proportional to the real part of the pN scattering amplitude. In the absence of short range correlations, $C_0 = 0$, the asymmetry stays negative valued at all p_m . It changes sign when correlation effects are included. In the latter case we can compare our results for 4He with the results for the deuteron, which should resemble each other. Indeed, for the soft and hard core correlations, both the

magnitude and p_m dependence of the asymmetry shown in Fig. 12 are remarkably similar to the forward backward asymmetry in $D(e, e'p)$ scattering [10]. For the deuteron target, the calculations are performed using the realistic wave functions which directly include the effects of short distance proton-neutron interaction. From this comparison we can conclude that, first, our simple Ansatz wave function correctly models gross features of short-distance nucleon-nucleon interaction in the ${}^4\text{He}$ and, second, the found change of the sign of $A_{FB}(p_m)$ and its rise with the correlation strength at large p_m are on firm grounds. It is this enhancement of $A_{FB}(p_m)$ which effectively cancels the effect of slight decrease of $W_+(p_m)$ and produces the correlation independent $W(\theta = 0^\circ; p_m)$. It is this enhancement of $A_{FB}(p_m)$ which amplifies the slight decrease of $W_+(p_m)$ and produces the counterintuitive substantial decrease of $W(\theta = 180^\circ, p_m)$ with the correlation strength C_0 . We checked that the (in)sensitivity of $W(\theta = 0^\circ, 180^\circ; p_m)$ to the correlation strength C_0 decreases with the value of ρ . Having established the origin of masking effects of FSI on $W(\vec{p}_m)$ in the longitudinal kinematics, we wish to point out that in the ${}^4\text{He}(e, e'p)$ reaction there is one spectator proton but there are two spectator neutrons. The direct experimental knowledge of ρ for the pn scattering is marginal; in our estimates of FSI effects we rely upon the dispersion theory calculations reviewed in [27]. Even if the uncertainties with the value of ρ can be eliminated by accurate measurements of $W_+(p_m)$, the sensitivity of this quantity to the value of C_0 is not sufficiently strong for a reliable separation of the ISC component of $N(p_m)$.

The overall conclusion from the above discussion is that, despite the FSI effects in the longitudinal kinematics being less striking than in the transverse kinematics, in no part of the phase space is an unambiguous extraction of the short range correlation component of the SPMD $N(\vec{p}_m)$ from the experimental data on missing momentum distribution $W(\vec{p}_m)$ possible.

6 On the convergence of the power expansion in ISC and FSI

In section 3 we already commented on the importance of higher order effects in the two-body correlation function $C(\vec{r}_i - \vec{r}_j)$. Roughly, the important terms of each order differ by a factor of $\left(\frac{r_c}{R_o}\right)^3$, i.e. by 0.6 for $r_c = 0.5fm$ and by 0.1 for $r_c = 0.6fm$. (Indeed, as Figs. 14,15 show, the rate of convergence for $r_c = 0.6fm$ is visibly slower than for $r_c = 0.5fm$.) However, there are also large combinatorial factors, which make the higher order terms non-negligible. In the PWIA case, the highest existent order is twelve, and the number of terms in the n -th order is $\binom{12}{n}$, so we have 66 second order terms compared to 495 terms of fourth order to 924 terms of sixth order and still 495 terms of eighth order. This is a reason why the contribution of sixth order terms to $N(p_m)$ is still non-negligible. As a general rule, for a specific term to be important at high p_m , it has to connect the two trajectories of the OBDM with correlations, i.e. it has to contain an interaction of the type $C^\dagger(\vec{r}_4 - \vec{r}_i)C(\vec{r}_4' - \vec{r}_i')$ (plus any number of other correlations between the spectator nucleons and/or the spectator and struck nucleon trajectories) and/or a cyclic chain of correlations, e.g. $C(\vec{r}_4 - \vec{r}_i)C(\vec{r}_i - \vec{r}_j)C(\vec{r}_4' - \vec{r}_j')$. To the leading order, only three of the possible 66 $C^\dagger C, CC, C^\dagger C^\dagger$ terms contribute at large p_m , and the percentage of important terms per order increases with the order. The above points are illustrated by a comparison of specific higher terms (30) and (31) with the leading term (29). The importance of higher order effects is still more enhanced when FSI is included. Here, the expansion (25) contains 2^{18} terms.

From the practical point of view, the major complication with FSI is that the longitudinal coordinate integrations and the corresponding Fourier transforms have to be carried out numerically. At $p_{m,z} = 0$, though, the rôle of the correlation and FSI terms in the expansion (25) is very similar, and so are the convergence properties. Here we first present the pure FSI effects in the absence of correlations, $C_0 = 0$. Fig. 13a shows the convergence of $W(\theta = 90^\circ, p_m)$ for transverse kinematics. In the exact calculation, the momentum distribution $W(\vec{p}_m)$ is positive valued, to the lowest odd orders in Γ^\dagger, Γ

one can run into negative valued $W(\vec{p}_m)$. To higher orders in FSI, one introduces attenuation of the proton wave which leads to a depletion of $W(\theta = 90^\circ, p_m)$. Although to the fourth-order approximation one finds the positive valued, and slowly decreasing, contribution (29) from the double incoherent elastic rescattering, which could have enhanced $W(\theta = 90^\circ; p_m)$ somewhat, its normalization is too small to have an appreciable impact on the p_\perp distribution in the considered region of p_m . The situation in parallel and anti-parallel kinematics is very similar, see Figs. 13b,c. Here the crucial point is that FSI generates the large- p_m tail in $W(\vec{p}_m)$ even in the absence of short range correlations. The convergence is good and the change from the fourth to sixth order is marginal. In the considered case, the precocious convergence in (anti)parallel kinematics is due to an absence of correlations, see below and the discussion in section 5.

The convergence of the expansion in the correlation function, which was quite slow already in the PWIA, worsens when correlations are included. To have some idea on the interplay of FSI and ISC terms, we show how $W(\vec{p}_m)$ evolves when the expansion (25) is truncated at terms $\sim \Gamma^k C^{N-k}$. In Figs. 14,15, we present the results only for even order N , because to odd orders one can run into negative valued $W(\vec{p}_m)$. The results for $N \geq 6$ include the numerically stronger FSI effects to all orders. For transverse kinematics, we find a convergence at large p_m only for $N \geq 10$. In parallel and antiparallel kinematics, the contribution from $N = 12$ is still non-negligible. Here a part of the problem is an unexpectedly strong FSI-ISC interference effect associated with the real part of the pN scattering amplitude, which exhibits a strong sensitivity to short range correlations. To summarize, these results demonstrate that estimates of the missing momentum distribution to lowest orders in the correlation function and in the quasideuteron approximation are too crude for making quantitative conclusions. For the soft core correlation, $C_0 = 0.5$, the convergence is much faster.

7 Implications for nuclear transparency studies

Nuclear effects in $A(e, e'p)$ scattering are often discussed in terms of the transparency ratio

$$T_A(\vec{p}_m) = \frac{W(\vec{p}_m)}{N(\vec{p}_m)}.$$

The above presented results strongly support the point that the FSI effects do not reduce to an overall renormalization of the observed missing momentum distribution by the nuclear attenuation factor, which is an often uncritically made assumption. Only at $p_m \approx 0$ the found $\approx 24\%$ depletion can be interpreted as a pure nuclear attenuation effect; at larger missing momenta, a strong interplay of the attenuation and distortion effects leads to a nuclear transparency $T_A(\vec{p}_m)$ which exhibits both much stronger depletion and "antishadowing" behaviour $T_A(\vec{p}_m) \gg 1$. This is clearly seen in Fig. 16, in which we show nuclear transparency for transverse, parallel and anti-parallel kinematics for the hard core correlation. In the latter two cases, nuclear transparency is very strongly affected by the real part of the pN scattering amplitude, the effect of which can not be interpreted in terms of attenuation altogether.

In the experimental determination of nuclear transparency one inevitably runs into a sort of vicious circle: What is measured experimentally is the FSI-distorted missing momentum distribution $W(\vec{p}_m)$ and one is forced to rely upon some model calculations of the PWIA distribution $N(\vec{p}_m)$. (Still further complications and extra model dependence will be involved if the experimentally measured cross section does not allow an integration over a sufficiently broad range of missing energy E_m .) To a certain extent, this model SPMD $N(\vec{p}_m)$ can be checked against the experimentally measured missing momentum distribution $W(\vec{p}_m)$, implicitly and/or explicitly assuming that the FSI effects can be factored out as an overall attenuation factor. The above presented results (see also [11]) very clearly show this is not the case and in large parts of the phase space such a poor man's evaluation of nuclear transparency can lead astray. Such a procedure was used, for instance, in an analysis of the data from the recent NE18 experiment [29]. Apart from the factorization assumption, in the NE18 analysis quite a large p_m -independent

renormalization was applied to the model SPMD $N(\vec{p}_m)$ in anticipation of the short-range correlation induced reshuffling of strength from the small to large missing momenta. Here we only wish to observe, that the results of section 3, see Fig. 5, cast a shadow on such an oversimplified treatment of the correlation effects.

Having performed a full analysis of the combined ISC and FSI effects and having established a primacy of FSI effects, we are in the position to address the question of how strongly nuclear transparency is sensitive to correlation effects. In Fig.16 we present a nuclear transparency calculated for different correlation strength,

$$T_A(C_0; \vec{p}_m) = \frac{W(C_0; \vec{p}_m)}{N(C_0; \vec{p}_m)}. \quad (35)$$

At large missing momenta, $p_m \gtrsim 1.5 \text{ fm}^{-1}$, the transparency becomes very sensitive to the correlation strength. In the region of moderate missing momenta, $p_m \lesssim 1.3 \text{ fm}^{-1}$, though, nuclear transparency exhibits hardly any sensitivity to the correlation strength, which confirms the anticipation in [11].

The experimental data are often presented in terms of a nuclear transparency ratio for the cross sections integrated over a certain momentum window. We present our results for the longitudinal and perpendicular partially integrated transparencies T_L and T_\perp defined as follows:

$$T_L(p_\perp = 0, p_z) = \frac{\int_0^{p_z} dp'_z W(p_\perp = 0, p'_z)}{\int_0^{p_z} dp'_z N(p_\perp = 0, p'_z)} \quad (36)$$

$$T_\perp(p_\perp, p_z = 0) = \frac{\int_0^{p_\perp} dp'_\perp p'_\perp W(p'_\perp, p_z = 0)}{\int_0^{p_\perp} dp'_\perp p'_\perp N(p'_\perp, p_z = 0)} \quad (37)$$

and the integrated transparency T_{int}

$$T_{int}(p_\perp) = \frac{\int_0^{p_\perp} dp'_\perp p'_\perp \int_{-\infty}^{\infty} dp_z W(p'_\perp, p_z)}{\int_0^{p_\perp} dp'_\perp p'_\perp \int_{-\infty}^{\infty} dp_z N(p'_\perp, p_z)}. \quad (38)$$

In agreement with the discussion in [31] the integrated transparencies are larger when correlation effects are included. However, the overall effect is very small confirming the conclusions of Ref. [32].

The size of the partially integrated transparencies $T_\perp(p_\perp)$ and $T_L(p_z)$ with the upper limit of integration p_\perp (p_z) is quite natural because the larger p_\perp (p_z), the larger fraction

of struck protons deflected by elastic scattering is included. What is not so obvious is that $T_{int}(p_{\perp} \sim 0)$ is not really smaller than the fully integrated transparency $T_{int}(\infty)$. The naive semiclassical expectation is that $1 - T_{int}(p_{\perp} \sim 0) \propto \sigma_{tot}(pN)$ vs. $1 - T_{int}(\infty) \propto \sigma_{in}(pN)$, because in counterdistinction to the former case in the latter case the deflection of struck protons by elastic rescatterings must not contribute to nuclear attenuation. This expectation is not born out by exact calculation, which demonstrates the pitfalls of the semiclassical treatment of $W(\vec{p}_m)$ and the importance of the point that FSI distortions do not admit the classical interpretation.

8 Discussion of the results and conclusions

Quasielastic $A(e, e'p)$ scattering at large missing momentum p_m is a natural place to look at the large- p_m component of the single-particle momentum distribution, which is expected to be generated by short range correlations of nucleons in the ground state of a target nucleus and which is well known to rise with the correlation strength. Our principal finding is that the large- p_m behavior of the observed missing momentum distribution in ${}^4\text{He}(e, e'p)$ is dominated by final state interaction of the struck proton with spectator nucleons and by the intricate interplay and quantal interference of the FSI and ground state correlation effects. In transverse kinematics, the FSI contribution to $W(\vec{p}_m)$ exceeds the ISC contribution to the SPMD by the order of magnitude. Even here, a substantial part of the FSI effect comes from a quantum mechanical FSI-ISC interference effect in the one body density matrix, which defies a semiclassical interpretation. The pattern of FSI-ISC interference effects is still more complex for longitudinal kinematics, where we found a novel effect of strong enhancement of the forward-backward asymmetry by short range correlations in the ground state. In antiparallel kinematics, this ISC-FSI interference effect in the contribution of the real part of the pN scattering amplitude leads to the FSI-modified $W(\vec{p}_m)$ which decreases with the correlation strength in the opposite to the SPMD. We are led to the conclusion that FSI effects make impossible a model-independent determination of the SPMD $N(\vec{p}_m)$ from the experimentally measured

missing momentum distribution $W(\vec{p}_m)$. Large FSI effects are of quite a generic origin and are not an artifact of the Ansatz wave function used in our evaluations, realistic though it is. We emphasize a simple and well understood origin of large enhancement parameters (27,30), which is a large radius of the nucleus as compared to a small radius of short range correlations. There remains the intriguing possibility of the forward-backward asymmetry as a probe of short range correlations and further studies of the model dependence of this observable are worth while.

Our Ansatz for the wave function was motivated by a desire to have a complete calculation of both short range correlation and final state interaction effects, rather than an evaluation of several lowest order terms. Even though much of the integrations and Fourier transforms can be performed analytically, the numerical calculations present quite a formidable task. The above presented results show that higher order correlation and FSI effects are indeed important. Our simple Jastrow function only includes the S -wave correlations. Our previous work on the missing momentum distribution for ${}^2H(e, e'p)$ scattering suggests that the D -wave effects are not that important [10, 12]. Specifically, it has been shown that the sensitivity to different models for the deuteron wave function, which give the D -wave contributions to $N(\vec{p}_m)$ differing at large p_m by an order of magnitude, is completely lost when including FSI. This insensitivity towards the D -wave is due to the fact that the FSI operator is short ranged and therefore does not affect the D -wave very much, as the D -wave is suppressed at small distances by the centrifugal barrier. At the higher missing momenta we are interested in, the missing momentum distribution was found to be dominated by FSI distortions of the S -wave contribution. Therefore, we can expect that the D -wave effects would not change our conclusions on the relative importance of the FSI and ISC effects at large p_m . One of the interesting findings is a substantial effect of higher order terms in the pair correlation function, which clearly shows an inadequacy of the oversimplified quasi-deuteron model for the large- p_m component of the missing momentum distribution, both in PWIA and with allowance for FSI.

One interesting implication of a dominance of FSI effects at large p_m in both ${}^2H(e, e'p)$

and ${}^4\text{He}(e, e'p)$ scattering is the similarity of missing momentum spectra (scaled up by the factor ~ 3 for the deuteron). Such a similarity emerges not because of the quasi-deuteron mechanism in the ${}^4\text{He}$, but because of the universality of final state proton-nucleon interaction in both nuclei [30].

Strong FSI effects in parallel kinematics also affect an interpretation of the y-scaling analysis of $(e, e'p)$ scattering in terms of the SPMD. To the extent that according to the experimental data, the FSI parameters - the total $p - n$ cross section, diffraction slope, the ratio ρ of real to imaginary part of the forward elastic scattering amplitude - vary only slightly for Q^2 of several GeV^2 , the FSI dominated $W(\vec{p}_m)$ also shall stay approximately Q^2 independent over the CEBAF range of Q^2 . This fact leads to an “FSI-scaling” effect that should not be confused with real y-scaling.

Last but not least it is well known that for the high density of ${}^4\text{He}$, the ISC-induced large- p_m tail of the SPMD does not change substantially from ${}^4\text{He}$ to heavy nuclei [17, 21, 22]. On the other hand, the FSI effects rise steeply with the mass number. For instance, the nuclear transparency decreases from ~ 0.75 for ${}^4\text{He}$ down to ~ 0.25 for ${}^{197}\text{Au}$ [29]. This suggests strongly that FSI distortions will be still stronger and ISC effects will become marginal in $A(e, e'p)$ on heavy nuclear targets.

Acknowledgments: We acknowledge discussions with S.Boffi, C.Ciofi degli Atti, S.Simula and J. Speth. This work was supported in part by the INTAS Grant No. 93-239 and by the Vigoni Program of DAAD (Germany) and the Conferenza Permanente dei Rettori (Italy). A.Bianconi thanks J.Speth for the hospitality at IKP, KFA Jülich, and S.Jeschonnek thanks S.Boffi for the hospitality at the University of Pavia.

References

- [1] A.E.I.Dieperink and P.K.A. de Witt Huberts, *Annu. Rev. Nucl. Part. Sci.* **40** (1990) 239; S.Boffi, C.Giusti and F.D.Pacati, *Phys.Rep.* **226** (1993) 1.
- [2] K.Gottfried, *Ann.Phys.* **21** (1963) 29; W.Czyż and K.Gottfried, *Nucl.Phys.* **21** (1961) 676; *Ann.Phys.* **21** (1963) 47.
- [3] N.Srivastava, *Phys.Rev.* **135B** (1964) 612; D.U.L.Yu, *Ann. Phys. (NY)* **38** (1966) 392.
- [4] J.W.Van Orden, W.Truex and M.K.Banerjee, *Phys. Rev.* **C21** (1980) 2628; S.Fantoni and V.R.Pandharipande, *Nucl. Phys.* **A427** (1984) 473; S.C.Pieper, R.B.Wiringa and V.R.Pandharipande, *Phys. Rev. C46* (1992) 1741.
- [5] J.Mougey (spokesperson), CEBAF Proposal No. E-89-044; R.G.Milner (spokesperson), CEBAF Proposal No. E-91-007; D.F.Geesaman (spokesperson), CEBAF Proposal No. E-91-011.
- [6] N.N.Nikolaev, A.Szczurek, J.Speth, J.Wambach, B.G.Zakharov and V.R.Zoller, *Nucl.Phys* **A582** (1995) 665.
- [7] N.N.Nikolaev, A.Szczurek, J.Speth, J.Wambach, B.G.Zakharov and V.R.Zoller, *Phys.Rev.* **C50** (1994) R1296.
- [8] J.Nemchik, N.N.Nikolaev and B.G.Zakharov, Proceedings of the Workshop on CEBAF at Higher Energies, CEBAF, April 14-16, 1994, Editors: Nathan Isgur and Paul Stoler, pp. 415-464.
- [9] A.Bianconi, S.Jeschonnek, N.N.Nikolaev and B.G.Zakharov, *Phys. Lett.* **B338** (1994) 123.

- [10] A.Bianconi, S.Jeschonnek, N.N.Nikolaev and B.G.Zakharov, *Phys. Lett.* **B343** (1995) 13.
- [11] N.N.Nikolaev, J.Speth and B.G.Zakharov, Jülich preprint **KFA-IKP(Th)-1995-1** (1995), submitted to *Nucl. Phys. A*.
- [12] A.Bianconi, S.Jeschonnek, N.N.Nikolaev and B.G.Zakharov, Jülich preprint **KFA-IKP(Th)-1995-02** (1995).
- [13] R.J.Glauber, in: *Lectures in Theoretical Physics*, v.1, ed. W.Brittain and L.G.Dunham. Interscience Publ., N.Y., 1959; R.J.Glauber and G.Matthiae, *Nucl. Phys.* **B21** (1970) 135.
- [14] J.G.Zabolitzky and W.Ey, *Phys. Lett.* **B76** (1978) 527.
- [15] S.Frullani and J.Mougey, *Adv. Nucl. Phys.*, Editors J.W.Negele and E.Vogt **14**, 3 (1984); G.Jacob and Th.A.J.Maris, *Rev.Mod. Phys.* **38** (1966) 121.
- [16] T. de Forest Jr., *Nucl.Phys.* **A392** (1983) 232.
- [17] C.Ciofi degli Atti, E.Pace and G.Salme, *Phys. Rev.* **C43** (1991) 1155.
- [18] M.Traini and G.Orlandini, *Z.Phys.A* **321** (1985) 479.
- [19] A.N.Antonov, P.E.Hodgson, and I.Zh.Petkov, *Nucleon Momentum and Density Distributions in Nuclei*, Clarendon Press, Oxford, 1988.
- [20] R.I.Dzhibuti and R.Ya.Kezerashvili, *Sov. J. Nucl. Phys.* **20** (1974) 17.
- [21] V.R.Pandharipande and S.C.Pieper, *Phys. Rev.* **C45** (1992) 791; R.Schiavilla, D.S.Lewart, V.R.Pandharipande, S.C.Pieper, R.B.Wiringa and S.Fantoni, *Nucl. Phys.* **A473** (1987) 267.
- [22] G.Có, A.Fabrocini and S.Fantoni, *Nucl. Phys.* **A568** (1994) 73.
- [23] H.de Vries, C.W. de Jager, and C. de Vries, *Atomic Data and Nuclear Data Tables* **36** (1987) 495.

- [24] R.B.Wiringa, *Nucl. Phys.* **A543** (1992) 199c.
- [25] G.D.Alkhozov, S.I.Belostotsky and A.A.Vorobyev, *Phys. Rep.* **C42** (1978) 89.
- [26] T.Lasinski et al., *Nucl. Phys.* **B37** (1972) 1.
- [27] C.Lechanoine-LeLuc and F.Lehar, *Rev. Mod. Phys.* **65** (1993) 47.
- [28] L.G.Dakhno and N.N.Nikolaev, *Nucl. Phys.* **A436** (1985) 653.
- [29] NE18 Collaboration: N.C.R.Makins et al., *Phys. Rev. Lett* **72** (1994) 1986; T.G. O'Neill et al., *Phys. Rev. C* (1995) in press; N.C.R.Makins and R.G.Milner, *preprint MIT-LNS 94-79*.
- [30] A.Bianconi, S.Jeschonnek, N.N.Nikolaev and B.G.Zakharov, Jülich preprint **KFA-IKP(Th)-1995-14** (1995).
- [31] O.Benhar, A.Fabrocini, S.Fantoni, V.R.Pandharipande, and I.Sick, *Phys. Rev. Lett.* **69** (1992) 881.
- [32] N.N.Nikolaev, A.Szczurek, J.Speth, J.Wambach, B.G.Zakharov and V.R.Zoller, *Phys. Lett.* **B317** (1993) 281.

Figure Captions

Figure 1: Schematic diagrams of several contributions to the one-body density matrix containing correlations. a) a linear correlation term of the type $C^\dagger(\vec{r}_i' - \vec{r}_4')$, b) the quadratic contribution $C^\dagger(\vec{r}_i' - \vec{r}_4') C(\vec{r}_i - \vec{r}_4)$ and c) a cyclic third order contribution of the type $C^\dagger(\vec{r}_4' - \vec{r}_i') C(\vec{r}_i - \vec{r}_k) C(\vec{r}_k - \vec{r}_4)$.

Figure 2: The single particle momentum distribution (SPMD) for the mean field distribution $C_o = 0$ (dotted curve), for soft core correlations $C_o = 0.5$ (dashed curve) and for hard core correlations $C_o = 1$ (solid curve). The other parameters are $R_o = 1.29 fm$ and $r_c = 0.5 fm$.

Figure 3: The single particle momentum distribution (SPMD) for different values of the correlation radius r_c . The solid curve shows $r_c = 0.5fm$ and the dashed curve shows $r_c = 0.6fm$. The other parameters are $R_o = 1.29fm$ and $C_o = 1$.

Figure 4: The convergence behaviour of the single particle momentum distribution for $R_o = 1.29fm$, $r_c = 0.5fm$ and $C_o = 1$. The dotted line includes all terms up to second order, the dashed line includes all terms up to fourth order, the dash-dotted line shows all terms up to sixth order, the double-dotted line includes all terms up to eighth order and the solid line shows the full calculation, i.e. it includes all terms up to twelfth order.

Figure 5: The pattern of renormalization of the SPMD for the short range correlation.

Figure 6: Schematic diagrams of several contributions to the one-body density matrix modified by final state interactions and correlations. Panel a) shows a linear final state interaction term of the type $\Gamma^\dagger(\vec{r}_i' - \vec{r}_4')$, panel b) shows the most important quadratic contribution $\Gamma^\dagger(\vec{r}_i' - \vec{r}_4') \Gamma(\vec{r}_i - \vec{r}_4)$ and panel c) shows a second order FSI-ISC interference contribution of the type $\Gamma^\dagger(\vec{r}_4' - \vec{r}_i') C(\vec{r}_i - \vec{r}_4)$.

Figure 7: The angular dependence of the missing momentum distribution $W(\vec{p}_m)$ for different missing momenta p_m (full line). For comparison, the corresponding value of the single particle momentum distribution $N(p_m)$ is also plotted (dotted line).

Figure 8: The missing momentum distribution $W(\vec{p}_m)$ (full line) and the single particle momentum distribution $N(p_m)$ (dashed line) for $\theta = 90^\circ$ (upper panel), $\theta = 0^\circ$ (middle panel), and for $\theta = 180^\circ$ (lower panel). The parameters for the nuclear ground state are $R_o = 1.29fm$, $r_c = 0.5fm$ and $C_o = 1$.

Figure 9: The missing momentum distribution $W(\vec{p}_m)$ is plotted for hard core correlations, $C_o = 1$, (solid line), soft core correlations, $C_o = 0.5$, (dashed line) and no correlations at all, $C_o = 0$ (dotted line), for different angles θ . The upper panel shows the results for $\theta = 90^\circ$, $\theta = 0^\circ$ is shown in the middle panel and $\theta = 180^\circ$ is shown in the lower panel. The other parameters are $R_o = 1.29fm$ and $r_c = 0.5fm$.

Figure 10: The same as in the previous figure, only with the correlation radius $r_c = 0.6fm$ instead of $r_c = 0.5fm$ as above.

Figure 11: The distribution $W_+(p_m) = \frac{1}{2}[W(\theta = 0^\circ; p_m) + W(\theta = 180^\circ)]$ is shown for hard core correlations, $C_o = 1$, (solid line), soft core correlations, $C_o = 0.5$, (dashed line) and no correlations at all, $C_o = 0$, (dotted line). The other parameters are $R_o = 1.29fm$ and $r_c = 0.5fm$. For comparison, the single particle momentum distribution for hard core correlations, $C_o = 1$, is also shown (dash-dotted line).

Figure 12: The forward-backward asymmetry $A_{FB}(p_m)$ as defined in (34) is shown for hard core correlations, $C_o = 1$, (solid line), soft core correlations, $C_o = 0.5$, (dashed line) and no correlations at all, $C_o = 0$, (dotted line). The other ground state parameters are $R_o = 1.29fm$ and $r_c = 0.5fm$.

Figure 13: The convergence behaviour of the missing momentum distribution $W(\vec{p}_m)$ without any correlations, i.e. $C_o = 0$, for different angles θ . The dotted line shows all the terms up to second order, the dashed line represents all terms up to fourth order, and the full line shows the complete result, i.e. all terms up to sixth order. The upper panel shows the results for $\theta = 90^\circ$, $\theta = 0^\circ$ is shown in the middle panel and $\theta = 180^\circ$ is shown in the lower panel. The other parameters are $R_o = 1.29fm$ and $r_c = 0.5fm$.

Figure 14: The convergence behaviour of the missing momentum distribution $W(\vec{p}_m)$ with hard core correlations, i.e. $C_o = 1$, for different angles θ . The dotted line shows all the terms up to second order, the dashed line represents all terms up to fourth order, the dash-dotted line shows all terms up to sixth order, the double-dotted line includes all terms up to eighth order, the long-dashed line shows the calculation up to the tenth order, the dash-double-dotted line represents all terms up to twelfth order, and the full line shows the complete result, i.e. all terms up to 18th order. The upper panel shows the results for $\theta = 90^\circ$, $\theta = 0^\circ$ is shown in the middle panel and $\theta = 180^\circ$ is shown in the lower panel. The other parameters are $R_o = 1.29fm$ and $r_c = 0.5fm$.

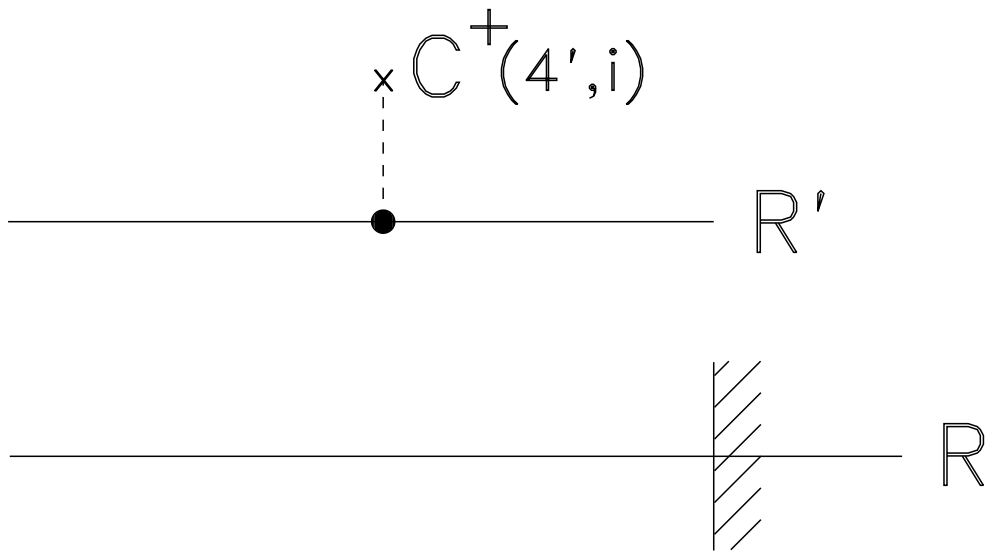
Figure 15: The convergence behaviour of the missing momentum distribution $W(\vec{p}_m)$ with soft core correlations, i.e. $C_o = 0.5$, for different angles θ . The dotted line shows all the terms up to second order, the dashed line represents all terms up to fourth order, the dash-dotted line shows all terms up to sixth order, the double-dotted line includes all terms up to eighth order, the long-dashed line shows the calculation up to the tenth order, the dash-double-dotted line represents all terms up to twelfth order, and the full line shows the complete result, i.e. all terms up to 18th order. The upper panel shows the results for $\theta = 90^\circ$, $\theta = 0^\circ$ is shown in the middle panel and $\theta = 180^\circ$ is shown in the lower panel. The other parameters are $R_o = 1.29fm$ and $r_c = 0.5fm$.

Figure 16: The nuclear transparency $T_A(\vec{p}_m)$ as defined in (35) is shown for hard core correlations, $C_o = 1$, (solid line), soft core correlations, $C_o = 0.5$, (dashed line) and no correlations at all, $C_o = 0$, (dotted line). The upper panel shows the results for $\theta = 90^\circ$, $\theta = 0^\circ$ is shown in the middle panel and $\theta = 180^\circ$ is shown in the lower panel. The other ground state parameters are $R_o = 1.29fm$ and $r_c = 0.5fm$.

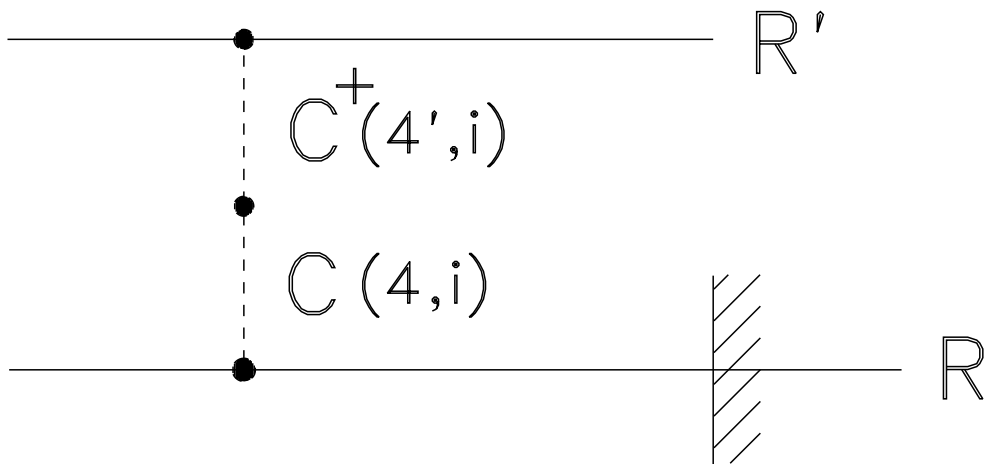
Figure 17: The ratios T_L (T_\perp) of the p_z (p_\perp) integrated spectral functions as function of the integration limit p_{max} as defined in (36), (37) are shown for hard core correlations, $C_o = 1$, (solid line), soft core correlations, $C_o = 0.5$, (dashed line) and no correlations at all, $C_o = 0$, (dotted line). The upper panel shows the results for $\theta = 90^\circ$, $\theta = 0^\circ$ is shown in the middle panel and $\theta = 180^\circ$ is shown in the lower panel. The other ground state parameters are $R_o = 1.29fm$ and $r_c = 0.5fm$.

Figure 18: The fully integrated transparency T_{int} as function of the integration limit $p_{\perp,max}$ as defined in (38) are shown for hard core correlations, $C_o = 1$, (solid line), soft core correlations, $C_o = 0.5$, (dashed line) and no correlations at all, $C_o = 0$, (dotted line). The other ground state parameters are $R_o = 1.29fm$ and $r_c = 0.5fm$.

a)



b)



c)

